Investigation of the nonlinear static and dynamic behaviour of rectangular microplates under electrostatic actuation

S. Saghir, M.I. Younis
4700 King Abdullah University of Science and Technology (KAUST), Thuwal 23955-6900, Saudi Arabia

Abstract. We present an investigation of the static and dynamic behavior of the nonlinear von-Karman plates when actuated by the nonlinear electrostatic forces. The investigation is based on a reduced order model developed using the Galerkin method, which rely on modeshapes and in-plane shape functions extracted using a finite element method. In this study, a fully clamped microplate is considered. We investigate the static behavior and the results are validated by comparison with the results calculated by a finite element model. The forced-vibration response of the plate is then investigated when the plate is excited by a harmonic AC load superimposed to a DC load. The dynamic behavior is examined near the primary resonance. The microplate shows a strong hardening behavior due to the cubic nonlinearity of mid-plane stretching. However, the behavior switches to softening as the DC load is increased.

1. Introduction

Micro-Electro Mechanical Systems (MEMS) commonly use electrically actuated flexible micro-structures, such as microbeams and microplates [1, 2]. Examples include pressure, mass and gas sensors, micropumps, microjets, micromirror, and microphones [3, 4]. Modeling accurately the mechanical behavior of such structures under the applied electric force is required to predict the response prior to the experimental testing and actual use of the device. Accurate models can guide the design engineer through the design process; reducing the design time on one hand and on the other hand can help to improve the existing devices. It is common to study the mechanical behavior of MEMS using linear theory [2]; which is applicable only for small deflections. Since in MEMS, structures often undergo large deflection, linear theory becomes inaccurate. Common modeling approaches include lumped mass models and Finite Element Method (FEM) [4, 5]. Lumped mass models give rough estimate of the response only. FEM based software tools are accurate but computationally expensive, especially when it comes to study the nonlinear dynamic behavior. On the other hand Reduced Order Models (ROM) based on the Galerkin approach have got popularity during the last decades because of their accuracy and low computational cost [6-10]. They have the capability to reveal the effect of different design parameters very conveniently.

A common way to model the plate structures in MEMS devices is using the linear plate theory [11-13], which is correct when out of plane deflection is small. But in cases when the transverse deflection is comparable to the thickness of the plate, a strong geometric nonlinearity is present due to mid-plane stretching making the predications of linear theories erroneous.

Most of the works reported in literature, have been mainly focused on the static and linear vibration behavior of microplates. Almost no work has been presented about the nonlinear behavior of microplates when actuated by large electrostatic loading or when undergoing large motion. Understanding such behaviors is fundamental to the development of the next generation microplates-based MEMS devices.

The objective of this paper is to investigate the nonlinear forced vibration behavior of electrically actuated fully clamped microplates. Towards this, we develop a reduced order model based on the von Karman equations of the plate, in which all three equations of the plate motion are discretized using the Galerkin method. For validation purpose, we compare the static results computed by the reduced order model with the results calculated using the FEM software COMSOL [14]. Further the reduced order model is employed to investigate the dynamic behavior of the plates under large vibration amplitude.

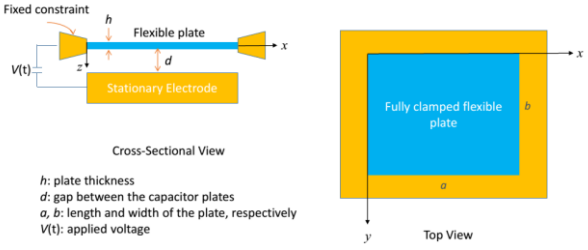

Fig. 1: A schematic diagram of an electrically actuated fully clamped microplate.

2. Problem Formulation

We consider a fully clamped rectangular microplate as shown in figure 1 and adopt the von-Karman equations of motion [15, 16]. We ignore the in-plane inertia since the in-plane natural frequencies are much higher than the transverse natural frequencies. Hence, the in-plane inertia has negligible effect on the transverse motion. Dropping the in plane inertia terms, the governing equations of the plate motion can be written as

$$\frac{\partial^2 u}{\partial x^2}+\frac{1}{2}(1+\upsilon)\frac{\partial^2 v}{\partial x\partial y}+\frac{1}{2}(1-\upsilon)\frac{\partial^2 u}{\partial y^2}+\frac{\partial w}{\partial x}\frac{\partial^2 w}{\partial x^2}+\frac{1}{2}(1+\upsilon)\frac{\partial w}{\partial y}\frac{\partial^2 w}{\partial x\partial y}+\frac{1}{2}(1-\upsilon)\frac{\partial w}{\partial x}\frac{\partial^2 w}{\partial y^2}=0 \quad (1)$$

$$\frac{\partial^2 v}{\partial y^2}+\frac{1}{2}(1+\upsilon)\frac{\partial^2 u}{\partial x\partial y}+\frac{1}{2}(1-\upsilon)\frac{\partial^2 v}{\partial x^2}+\frac{\partial w}{\partial y}\frac{\partial^2 w}{\partial y^2}+\frac{1}{2}(1+\upsilon)\frac{\partial w}{\partial x}\frac{\partial^2 w}{\partial x\partial y}+\frac{1}{2}(1-\upsilon)\frac{\partial w}{\partial y}\frac{\partial^2 w}{\partial x^2}=0 \quad (2)$$

$$\begin{aligned}&\frac{h^2}{12}\nabla^4 w+\frac{\rho(1-\upsilon^2)}{Eh}\frac{\partial^2 w}{\partial t^2}+\frac{c(1-\upsilon^2)}{Eh}\frac{\partial w}{\partial t}=\frac{\varepsilon(1-\upsilon^2)V(t)^2}{2Eh(d-w)^2}\\&+\frac{(1-\upsilon^2)}{Eh}\left(N_{xx}\frac{\partial^2 w}{\partial x^2}+2N_{xy}\frac{\partial^2 w}{\partial x\partial y}+N_{yy}\frac{\partial^2 w}{\partial y^2}\right)\\&+\frac{\partial u}{\partial x}\left(\frac{\partial^2 w}{\partial x^2}+\upsilon\frac{\partial^2 w}{\partial y^2}\right)+\frac{\partial v}{\partial y}\left(\upsilon\frac{\partial^2 w}{\partial x^2}+\frac{\partial^2 w}{\partial y^2}\right)\\&+(1-\upsilon)\left(\frac{\partial u}{\partial y}+\frac{\partial v}{\partial x}\right)\frac{\partial^2 w}{\partial x\partial y}+\frac{1}{2}\left(\frac{\partial w}{\partial x}\right)^2\left(\frac{\partial^2 w}{\partial x^2}+\upsilon\frac{\partial^2 w}{\partial y^2}\right)\\&+\frac{1}{2}\left(\frac{\partial w}{\partial y}\right)^2\left(\upsilon\frac{\partial^2 w}{\partial x^2}+\frac{\partial^2 w}{\partial y^2}\right)+(1-\upsilon)\left(\frac{\partial w}{\partial x}\frac{\partial w}{\partial y}\frac{\partial^2 w}{\partial x\partial y}\right)\end{aligned} \quad (3)$$

where u, v and w are the displacements along the x, y and z direction, respectively, ∇^4 is the bi-harmonic operator, $\nabla^4=\frac{\partial^4}{\partial x^4}+2\frac{\partial^4}{\partial x^2\partial y^2}+\frac{\partial^4}{\partial y^4}$, ρ is the mass density per unit area, c is the damping coefficient, and υ and E are Poisson's ratio and modulus of elasticity, respectively. The first term on the right side of equation (3) i.e. $\frac{\varepsilon(1-\upsilon^2)V(t)^2}{2Eh(d-w)^2}$ is the applied electric pressure in the transverse direction while N_{ij} is the applied force per unit length on the edge perpendicular to i^{th} axis in the j^{th} direction.

For convenience, we introduce the non-dimensional variables (denoted by hats);

$$\hat{x}=\frac{x}{a},\ \hat{y}=\frac{y}{b},\ \hat{w}=\frac{w}{d},\ \hat{u}=\frac{au}{d^2},\ \hat{v}=\frac{av}{d^2},\ \hat{t}=\frac{t}{T} \quad (4)$$

Substituting equation (4) into equations (1)-(3) and dropping the hats for convenience we get the following equations:

$$\frac{\partial^2 u}{\partial x^2}+\frac{(1+\upsilon)}{2\alpha}\frac{\partial^2 v}{\partial x\partial y}+\frac{(1-\upsilon)}{2\alpha^2}\frac{\partial^2 u}{\partial y^2}+\frac{\partial w}{\partial x}\frac{\partial^2 w}{\partial x^2}+\frac{(1+\upsilon)}{2\alpha^2}\frac{\partial w}{\partial y}\frac{\partial^2 w}{\partial x\partial y}+\frac{(1-\upsilon)}{2\alpha^2}\frac{\partial w}{\partial x}\frac{\partial^2 w}{\partial y^2}=0 \quad (5)$$

$$\frac{\partial^2 v}{\partial y^2}+\frac{(1+\upsilon)\alpha}{2}\frac{\partial^2 u}{\partial x\partial y}+\frac{(1-\upsilon)\alpha^2}{2}\frac{\partial^2 v}{\partial x^2}+\frac{1}{\alpha}\frac{\partial w}{\partial y}\frac{\partial^2 w}{\partial y^2}+\frac{(1+\upsilon)\alpha}{2}\frac{\partial w}{\partial x}\frac{\partial^2 w}{\partial x\partial y}+\frac{(1-\upsilon)}{2}\frac{\partial w}{\partial y}\frac{\partial^2 w}{\partial x^2}=0 \quad (6)$$

$$\begin{aligned}&\frac{\partial^4 w}{\partial x^4}+\frac{2}{\alpha^2}\frac{\partial^4 w}{\partial x^2\partial y^2}+\frac{1}{\alpha^4}\frac{\partial^4 w}{\partial y^4}+\frac{\partial^2 w}{\partial t^2}+\hat{c}\frac{\partial w}{\partial t}=\alpha_2\frac{V(t)^2}{(1-w)^2}\\&+3\alpha_0^2\left\{\hat{N}_{xx}\frac{\partial^2 w}{\partial x^2}+\frac{2}{\alpha}\hat{N}_{xy}\frac{\partial^2 w}{\partial x\partial y}+\frac{1}{\alpha^2}\hat{N}_{yy}\frac{\partial^2 w}{\partial y^2}\right\}\\&+12\alpha_1^2\left\{\begin{aligned}&\frac{\partial u}{\partial x}\left(\frac{\partial^2 w}{\partial x^2}+\frac{\upsilon}{\alpha^2}\frac{\partial^2 w}{\partial y^2}\right)+\frac{1}{\alpha}\frac{\partial v}{\partial y}\left(\upsilon\frac{\partial^2 w}{\partial x^2}+\frac{1}{\alpha^2}\frac{\partial^2 w}{\partial y^2}\right)\\&+(1-\upsilon)\left(\frac{1}{\alpha}\frac{\partial u}{\partial y}+\frac{\partial v}{\partial x}\right)\frac{1}{\alpha}\frac{\partial^2 w}{\partial x\partial y}\end{aligned}\right\}\\&+12\alpha_1^2\left\{\begin{aligned}&\frac{1}{2}\left(\frac{\partial w}{\partial x}\right)^2\left(\frac{\partial^2 w}{\partial x^2}+\frac{\upsilon}{\alpha^2}\frac{\partial^2 w}{\partial y^2}\right)\\&+\frac{1}{2\alpha^2}\left(\frac{\partial w}{\partial y}\right)^2\left(\upsilon\frac{\partial^2 w}{\partial x^2}+\frac{1}{\alpha^2}\frac{\partial^2 w}{\partial y^2}\right)+\frac{(1-\upsilon)}{\alpha^2}\left(\frac{\partial w}{\partial x}\frac{\partial w}{\partial y}\frac{\partial^2 w}{\partial x\partial y}\right)\end{aligned}\right\}\end{aligned} \quad (7)$$

The parameters appearing in equations (5)-(7) are

$$\alpha=\frac{b}{a},\ \alpha_0=\frac{a}{h},\ \alpha_1=\frac{d}{h},\ \alpha_2=\frac{6(1-\upsilon^2)}{Eh^3d^3}\varepsilon a^4,\ \hat{c}=\frac{ca^4}{TD}$$

and $\hat{N}_{ij}=\frac{(1-\upsilon^2)}{Eh}N_{ij}$ (8)

where $T=\sqrt{\frac{\rho a^4}{D}}$ and $D=\frac{Eh^3}{12(1-\nu^2)}$.

3. Reduced Order Model

To develop the reduced order model for the governing equations (5)-(7), we assume the solution for the transverse and in-plane displacements as follows

$$w=\sum_{i=1}^{n}q_i(t)\phi_i(x,y) \quad (9)$$

$$u=q_u(t)\psi_u(x,y) \quad (10)$$

$$v=q_v(t)\psi_v(x,y) \quad (11)$$

where $\phi_i(x,y)$ are the transversal linear modeshapes of the plate and $q_i(t)$ are the unknown time dependent coefficients, $\psi_u(x,y)$ and $\psi_v(x,y)$ are the shape functions for the in-plane displacements u and v, while $q_u(t)$ and $q_v(t)$ are the corresponding time dependent unknown coefficients.

Since the linear eigenvalue problem governing the transversal linear modeshapes of the fully clamped plate cannot be solved analytically, we resort to the finite element method for this purpose. We use the commercial software COMSOL [14] to obtain the modeshapes of the plate. The in-plane displacement shape functions are also obtained by FEM while the plate is deflected by a uniform transverse pressure.

To treat the electric force term we multiply equation (7) by $(1-w)^2$ so that electric force term is represented exactly [6, 17]. Substituting equations (9)-(11) into equations (5)-(7), multiplying equation (5) and (6) by $\psi_u(x,y)$ and $\psi_v(x,y)$, respectively, and equation (7) by $\phi_i(x,y)$, and integrating over the plate domain, we get a system of differential algebraic equations (DAEs) for the time dependent coefficients. Equations (5) and (6) generate algebraic equations while equation (7) results in ordinary differential equations (ODEs). The resulting system of DAEs is solved for the unknown time dependent coefficients $q_i(t)$, $q_u(t)$ and $q_v(t)$. Toward this, we solve equations (5) and (6) for $q_u(t)$ and $q_v(t)$ in terms of $q_i(t)$ and then substitute the results into equation (7). This equation is then integrated in time using Runge Kutta method. These coefficients are substituted back into equations (9)-(11) to get the displacements w, u and v.

4. Static Analysis

To calculate the static deflection of the microplate under a DC load, we drop the time derivatives in the reduced order model and the time dependent unknown coefficients $q_i(t)$, $q_u(t)$, and $q_v(t)$ are replaced by constant coefficients q_i, q_u, and q_v. This results in a system of nonlinear algebraic equations, which is numerically solved for q_i, q_u and q_v. Then equation (9) is used to find the transversal deflection.

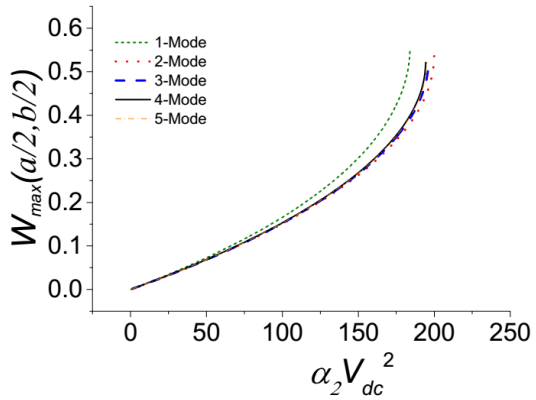

Fig. 2: Convergence of the static response with the number of transverse modes retained in the reduced order model. Variation of the maximum non-dimensional deflection $W_{\max}$ with the electrostatic voltage parameter $\alpha_2 V_{dc}^2$ when $\alpha=1$ and $\alpha_1=1$.

First we study convergence of the static results with the number of transverse modes, $\phi_i(x,y)$ retained in the reduced order model. Figure 2 shows the stable solution, the non-dimensional deflection $W_{\max}$ at the center of plate against various values of $\alpha_2 V_{dc}^2$. We note that the static results converge by retaining at least four transverse modes in the model. One can note that the deflection curve is limited by the pull-in instability, where the slope of the curve approaches infinity.

Next we validate the reduced order model by comparing its results with the results obtained by FEM software COMSOL [14] for different aspect ratios α. Figure 3 shows the maximum deflection $W_{\max}$ at the center of the microplate calculated by both models. We use rectangular microplates of four different aspect ratios of $\alpha=1$, $\alpha=1.1$, $\alpha=1.2$, and $\alpha=1.5$. Dimensional specifications of the electrically actuated microplates are given in Table 1, while material properties are; $E=153$GPa and $\upsilon=0.23$.

Table 1: Dimensional specifications of electrically actuated microplates used in the model validation.

Aspect ratio $\alpha=b/a$	Length $a(\mu m)$	Width $b(\mu m)$	Thickness $h(\mu m)$	Capacitor gap $d(\mu m)$
1	300	300	2	2
1.1	300	330	2	2
1.2	300	360	2	2
1.5	300	450	2	2

Results are shown for various values of V_{dc}, until the pull in instability, for $\alpha=1.5$. It shows excellent agreement among the results calculated by the ROM model and the FEM model.

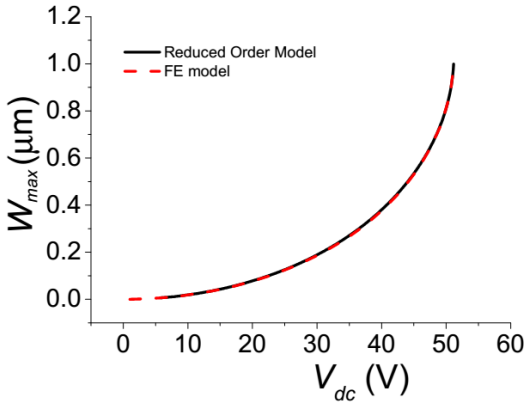

Fig. 3: Comparison of the maximum deflection $W_{\max}$ at the center of the microplate, calculated by the reduced order with the results obtained from FEM for various values of V_{dc} until the pull-in instability, for a rectangular microplate of aspect ratio $\alpha=1.5$.

5. Dynamic Analysis

In this section we investigate the dynamic response of the square microplate in the neighborhood of primary, resonances of the fundamental mode. We analyze the dynamics of the microplate by generating frequency response curves. The Runge Kutta method is used to perform long time numerical integration to solve the system of DAEs. The stable steady solution is captured after making sure that the transient response is no longer contributing to the response. Figure 4 shows the time history of the dynamic response of the microplate when actuated at $V_{dc}=3$V and $V_{ac}=0.1$V and $\Omega=35.1$. Figure 4a depicts the diminishing transient response, while figure

4b shows the stable steady state response. We use steady-state responses similar to figure 4b to construct the frequency response curves.

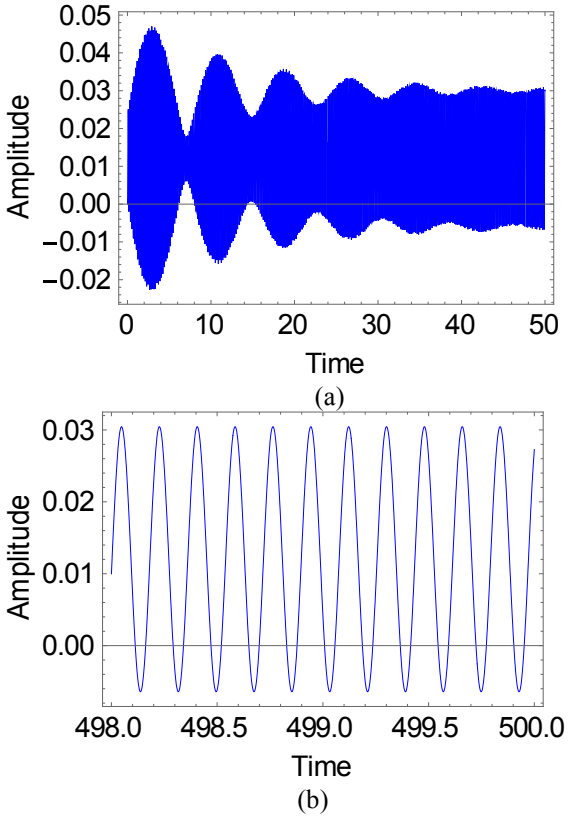

Fig. 4: Time history response of the microplate. (a) Transient response. (b) Steady state response.

To investigate the dynamic response at primary resonance, we fix $\alpha = 1$, $\alpha_1 = 1$, $\alpha_2 = 1$ and assume that the in-plane external forces are zero i.e. $N_{xx} = N_{xy} = N_{yy} = 0$. With the above parameters the static pull-in voltage for the microplate is near 14 Volts. We investigate the nonlinear dynamic behavior of the microplate near primary resonance, a small harmonic V_{ac} is superimposed to a V_{dc} i.e. $V(t) = V_{dc} + V_{ac} Sin(\Omega t)$. Figure 5 shows the nonlinear response of the microplate when actuated at $V_{dc} = 3\text{V}$ for various values of V_{ac} while the quality factor is fixed at $Q = 250$ near primary resonance, which for the linear plate is near 36. Our choice of a constant value of Q means that we assumed negligible effect of squeeze-film damping, which reasonable assumption is assuming that the microplate is placed inside a vacuum chamber and is operated at reduced pressure. Otherwise, squeeze-film damping can have strong effect on the dynamics of microplates and needs to be modeled using Reynolds equation and a structural-fluidic model [17, 18].

The microplate exhibits strong hardening effect due to the cubic nonlinearity, which comes into play due to mid-plane stretching. The hysteresis in the curves is captured by performing forward and backward frequency sweeps. Nonlinear resonance peaks occur near $\Omega = 36.15$ for $V_{ac} = 0.1\text{V}$ while it is at $\Omega = 36.6$ for $V_{ac} = 0.3\text{V}$ and $\Omega = 36.9$ for $V_{ac} = 0.5\text{V}$. Further we notice that there exist multiple stable solutions over some range of frequency and amplitude jumps from higher to lower or lower to higher values depending on the type of frequency sweep.

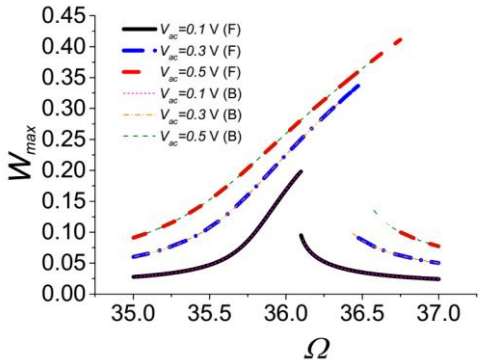

Fig. 5: Maximum non-dimensional deflection $W_{\max}$ at the center of the microplate against the actuating frequency Ω when actuated at $V_{dc} = 3\text{V}$ and various values of V_{ac} while quality factor $Q = 250$; (F) Forward frequency sweep, (B)Backward frequency sweep.

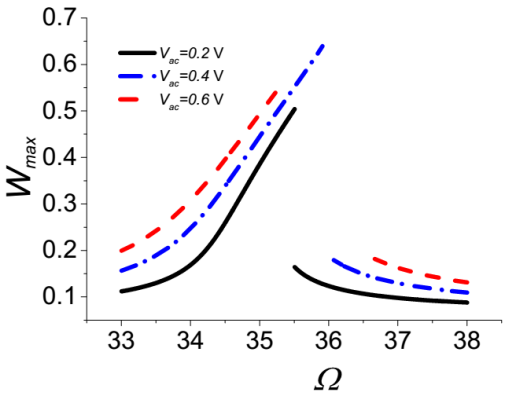

Fig. 6: Maximum non-dimensional deflection $W_{\max}$ of the microplate against the actuating frequency Ω when actuated at $V_{dc} = 7\text{V}$ and various values of V_{ac} while quality factor $Q = 250$.

Figure 6 shows the frequency response curves of the microplate when actuated at $V_{dc} = 7\text{V}$ for various values of V_{ac} with a quality factor $Q = 250$. An overlap of stable solutions exists when actuated at $V_{ac} = 0.2\text{V}$ contrary to the responses at $V_{ac} = 0.4\text{V}$ and $V_{ac} = 0.6\text{V}$, respectively. A gap between the two stable solutions starts to emerge in the case of $V_{ac} = 0.4\text{V}$ by the forward and backward frequency sweeps. This gap might indicate that the microplate becomes unstable at that actuating voltage and pulls on the stationary electrode. This kind of instability is called dynamic pull-in instability, which usually occurs at a lower DC load superimposed to a small harmonic load [17, 19-21]. Another possibility exists, especially in the case of $V_{ac} = 0.4\text{V}$, that this gap is created due to the numerical divergence of the time integration scheme, due to its inability to find suitable initial conditions that lead to

a stable periodic orbit. In other words, this might indicate highly fractal behavior, which usually gets stronger as the system approaches the dynamic pull-in regime [20]. To confirm if this divergence is due to fractal behavior or due to pull-in exactly, one should resort to other numerical techniques to find periodic motions, such as shooting and finite difference methods as well as basin of attraction analysis [17, 21]. The response on the other hand for the case of $V_{ac} = 0.6\text{V}$ is most likely an indication of a pull-in band, since as reported in [21], further increase in V_{ac} widens the pull-in band gap between the stable solutions and makes the upper stable branches terminated at lower values [21].

6. Conclusions

In this article we developed a reduced order model for the investigation of the static as well as the dynamic behavior of electrically actuated rectangular microplates. First convergence of the static results with the number of modeshapes retained in the ROM has been studied. We found that four modes are sufficient for convergence. The dynamic behavior of the microplate has been investigated near primary resonance using long time numerical integration. We captured the stable solutions using forward and backward frequency sweeps. The microplate actuated near primary resonance shows a strong hardening behavior due to the cubic nonlinearity, which comes into play due to mid-plane stretching. Increasing V_{ac} further widens the gap between the two stable solutions captured by forward and backward frequency sweeps and pull-in instability occurs at a lower vibration amplitude.

References

1. Chuang, W.C., H.L. Lee, P.Z. Chang, and Y.C. Hu, *Review on the modeling of electrostatic MEMS.* Sensors, 2010. **10**(6): p. 6149-6171.
2. Batra, R.C., M. Porfiri, and D. Spinello, *Review of modeling electrostatically actuated microelectromechanical systems.* Smart Materials and Structures, 2007. **16**(6): p. R23.
3. Tong, P. and W. Huang, *Large Deflection of Thin Plates in Pressure Sensor Applications.* Journal of Applied Mechanics, 2002. **69**(6): p. 785-789.
4. Ng, T.Y., T.Y. Jiang, H. Li, K.Y. Lam, and J.N. Reddy, *A coupled field study on the non-linear dynamic characteristics of an electrostatic micropump.* Journal of Sound and Vibration, 2004. **273**(4–5): p. 989-1006.
5. Pursula, A., P. Råback, S. Lähteenmäki, and J. Lahdenperä, *Coupled FEM simulations of accelerometers including nonlinear gas damping with comparison to measurements.* Journal of Micromechanics and Microengineering, 2006. **16**(11): p. 2345-2354.
6. Younis, M.I., E.M. Abdel-Rahman, and A. Nayfeh, *A reduced-order model for electrically actuated microbeam-based MEMS.* Microelectromechanical Systems, Journal of, 2003. **12**(5): p. 672-680.
7. Zhao, X., E.M. Abdel-Rahman, and A.H. Nayfeh, *A reduced-order model for electrically actuated microplates.* Journal of Micromechanics and Microengineering, 2004. **14**(7): p. 900-906.
8. Vogl, G.W. and A.H. Nayfeh, *A reduced-order model for electrically actuated clamped circular plates.* Journal of Micromechanics and Microengineering, 2005. **15**(4): p. 684-690.
9. Batra, R.C., M. Porfiri, and D. Spinello, *Reduced-order models for microelectromechanical rectangular and circular plates incorporating the Casimir force.* International Journal of Solids and Structures, 2008. **45**(11–12): p. 3558-3583.
10. Nayfeh, A.H., M.I. Younis, and E.M. Abdel-Rahman, *Reduced-order models for MEMS applications.* Nonlinear Dynamics, 2005. **41**(1-3): p. 211-236.
11. Machauf, A., Y. Nemirovsky, and U. Dinnar, *A membrane micropump electrostatically actuated across the working fluid.* Journal of Micromechanics and Microengineering, 2005. **15**(12): p. 2309-2316.
12. Chao, P.C., C.-W. Chiu, and C. Tsai, *A novel method to predict the pull-in voltage in a closed form for micro-plates actuated by a distributed electrostatic force.* Journal of Micromechanics and Microengineering, 2006. **16**(5): p. 986-998.
13. Nayfeh, A.H. and M.I. Younis, *A new approach to the modeling and simulation of flexible microstructures under the effect of squeeze-film damping.* Journal of Micromechanics and Microengineering, 2004. **14**(2): p. 170-181.
14. COMSOL, *http://www.comsol.com/*.
15. Nayfeh, A.H. and D.T. Mook, *Nonlinear oscillations*. 2008: John Wiley & Sons.
16. Nayfeh, A.H. and P.F. Pai, *Linear and nonlinear structural mechanics*. 2008: John Wiley & Sons.
17. Younis, M.I., *MEMS Linear and Nonlinear Statics and Dynamics: Mems Linear and Nonlinear Statics and Dynamics*. Vol. 20. 2011: Springer.
18. Younis, M.I. and A.H. Nayfeh, *Simulation of squeeze-film damping of microplates actuated by large electrostatic load.* Journal of Computational and Nonlinear Dynamics, 2007. **2**(3): p. 232-241.
19. Alsaleem, F.M., M.I. Younis, and H.M. Ouakad, *On the nonlinear resonances and dynamic pull-in of electrostatically actuated resonators.* Journal of Micromechanics and Microengineering, 2009. **19**(4): p. 045013.
20. Alsaleem, F.M., M. Younis, and L. Ruzziconi, *An experimental and theoretical investigation of dynamic pull-in in MEMS resonators actuated electrostatically.* Microelectromechanical Systems, Journal of, 2010. **19**(4): p. 794-806.
21. Nayfeh, A.H., M.I. Younis, and E.M. Abdel-Rahman, *Dynamic pull-in phenomenon in MEMS resonators.* Nonlinear Dynamics, 2007. **48**(1-2): p. 153-163.